Mechanical Systems and Signal Processing 133 (2019) 106280

Contents lists available at ScienceDirect

Mechanical Systems and Signal Processing

journal homepage: www.elsevier.com/locate/ymssp

Design of structural monitoring sensor network using surrogate modeling of stochastic sensor signal

Amin Toghi Eshghi [a], Soobum Lee [a,*], HyunJun Jung [b], Pingfeng Wang [c]

[a] Department of Mechanical Engineering, University of Maryland, Baltimore County, Baltimore, MD 21250, USA
[b] Department of Mechanical Engineering, Virginia Polytechnic Institute and State University, Blacksburg, VA 24061, USA
[c] Department of Industrial and Enterprise Systems Engineering, University of Illinois at Urbana-Champaign, Champaign, IL 61820, USA

ARTICLE INFO

Article history:
Received 23 October 2018
Received in revised form 17 July 2019
Accepted 25 July 2019
Available online 7 August 2019

Keywords:
Reliability-based design optimization
Probabilistic sensing
Mahalanobis Distance
Kriging modeling

ABSTRACT

Efficient Structural Health Monitoring (SHM) could reduce operation and maintenance costs, improve longevity, and enhance safety of the performance in complex mechanical systems. Traditional sensor network for SHM relied on simple sensor behavior without considering uncertain factors from system and environment. A probabilistic sensing model is required to simulate the realistic and stochastic sensor performance in the sensor network design process. In this paper, we introduce reliability-based design optimization for piezoelectric sensor network considering the detectability of different failure modes. The proposed method diagnoses failure based on the Mahalanobis Distance (MD) suitable for many SHM processes, while considering the uncertainties from structure properties and operation condition. Kriging is applied for surrogate modeling of the stochastic sensor signal and reduce computational cost. The optimal piezoelectric sensor network design is prototyped and its failure detection capability is experimentally verified.

1. Introduction

A low cost and reliable monitoring system has received more attention to ensure the safety and functionality of mechanical structures. Structural health monitoring (SHM) techniques based on the use of piezoelectric materials have attracted considerable attention. However, piezoelectric sensing technologies usually need large number of distributed sensors to perform the required monitoring process. Moreover, various sources of uncertainty from structure properties, external loading, and environmental condition changes may adversely affect the functionality of SHM sensors. One important aspect of smart sensing is to overcome these shortcomings by determining the optimum number and proper placement of the sensors on the structure.

Several studies have proposed different methodologies for determining the optimal location of piezoelectric actuators and sensors. A thorough review of optimization criteria for placement of piezoelectric sensors and actuators for structure monitoring is reported by Gupta et al. [1] that introduces methods of maximizing different objectives such as modal forces, deflection of the host structure, dissipated energy, degree of controllability, or degree of observability. It could also be defined to minimize the control energy or spill-over effect. For example, Lee et al. [2] searched for optimal sensor locations by maximizing the dissipation energy from the feedback control system. They used a quasi-Newtonian algorithm to solve the optimization problem. Zhang et al. [3] developed a float-encoded genetic algorithm for the optimal control of flexible smart

* Corresponding author.
E-mail address: sblee@umbc.edu (S. Lee).

https://doi.org/10.1016/j.ymssp.2019.106280
0888-3270/

structures on which piezoelectric sensors are bonded. This algorithm finds optimal sensor locations and feedback gains to maximize dissipation energy. Some other studies have developed optimization techniques based on controllability and observability analysis [4–6].

Another group of research is focused on pure optimization algorithm for optimal sensor placement (OSP) problems. Flynn and Todd [7] used Bayesian approach to derive a global optimality criterion within a detection theory framework. The optimal configuration was found by minimizing the total presence of either type I (false positives: when the monitoring system flags damage when in fact it is not) or type Π error (false negatives: when the monitoring system misses damage when it is damaged). They demonstrated the capability of this method for active sensing using guided ultrasonic waves. Cha et al. [8] showed a possible use of a multi-objective genetic algorithm (MOGA) to generate Pareto front curves for optimal placement of sensors. Sunar and Rao [9] implemented the quasistatic thermo-piezoelectricity equations and optimized the location of the thermo-piezoelectric sensors on cantilever beam structures. Since their method relies on the gradient of the objective function, it is highly probable to fall into the local optimum. Overton and Worden [10] applied the Ant Colony metaphor (ANCO) in combination with neural network for impact detection in a plate. Hernandez [11] developed an algorithm for unmeasured excitations and noise contaminated measurements within the context of Kalman filter to minimize the variance of state estimation error among possible sequential sensor locations. In some research [12,13] sparsity theory is used as the baseline for sensor network design. This scheme leverages sparsity to recover a sparse signal of interest as a solution of several surrogate minimization problems. Only a few studies have been focused on the numerical simulation for OSP problems that incorporate the structural uncertainties. Guratzsch and Mahadevan [14] developed a probabilistic finite element analysis (FEA) model to quantify sensor output for all possible locations. They executed deterministic FEA multiple times using statistical model inputs to realize performance uncertainty, but this approach requires high computational cost. Wang et al. [15] developed a reliability based robust design optimization for failure diagnosis using piezoelectric materials. Castro-Triguero et al. [16] considered modal analysis of a truss bridge and examined the influence of parametric uncertainties on the OSP. They assessed the optimal location of sensor with three different criteria: the Fisher matrix determinant, the modal assurance criterion error, and the condition number. Using all different methods, they concluded that the parametric uncertainties have significant influence on the optimal sensor location. Vincenzi and Simonini [17] investigated the effect of errors and parametric uncertainties in the optimal sensor location. They considered both parametric uncertainties and model uncertainties, and they applied Information Entropy theory to find the optimum solution based on the covariance matrix of prediction error. Dhillon and Chakarabarty [18] considered probabilistic sensor detection constraints to optimize the sensor placement with the minimum number of required sensors. Kirkegaard and Brincker [19] considered random variables to define the OSP. The results revealed that the optimal location of sensors becomes less sensitive to the noise-to-signal ratio as the number of sensors increases. Li and Kiureghian [20] combined maximum expected utility theory and a Bayesian linear layout to consider model and loading uncertainty into the OSP problem. The utility function was defined based on three criteria: quadratic loss, Shannon information, and K–L divergence. They applied this method for a 16-degrees-of-freedom shear-type building where underground motion and wind load were considered. It was concluded that the number of sensors should be equal to or more than the number of modes of interest.

Although the issue of structural health monitoring has been addressed in the literature, problems such as low sensitivity of failure detection, computational difficulties, high statistical uncertainty from structure are major hindrances in developing practical failure detection methods. In this paper we introduce a new probabilistic technique for optimal sensor placement (OSP) by detectability measure. Detectability means the ability of sensor network that distinguishes different health status, and is formulated using Mahalanobis Distance (MD). A practical solution is demonstrated to overcome the computational burdens via surrogate modeling of the stochastic performance of the system. This approach is verified for a piezoelectric sensor network problem with experiment. This article is organized as follows. In Section 2, probabilistic detectability concepts including probability of detection (PoD) and Mahalanobis Distance (MD) are discussed. In Section 3, use of kriging for surrogate modeling is explained. Section 4 represents reliability-based design optimization (RBDO) for the sensor network design. Section 5 describes a case study that considers the proposed method for health monitoring of skin panel structures as well as experimental verification. Section 6 concludes this paper.

2. Probabilistic detectability

Prognostics, diagnostics and health management are inevitable for reliable performance in any complex engineered systems. The approaches for SHM can be categorized into three sections, namely model-based, data-based, and hybrid approaches [21]. In all these methods, acquired data needs to be processed to understand their statistical characteristics and classified into different health status (HS). The crucial step is to adopt an appropriate algorithm to achieve a reliable health monitoring system especially when sensor noise and uncertainties related to system operating condition is involved. Numerous algorithms have been introduced to estimate the HS of the structure by classifying the signals in a supervised or unsupervised manner. Statistical inference-based algorithms such as Mahalanobis Distance [22], k-nearest neighbor [23], and k-mean clustering [24] are frequently used to classify system HSs. MD is used for classifying the data where it accounts for the variance of each variable and the covariance between variables. MD is very efficient for detecting outliers and suitable for dividing large amount of multivariate data into different classes. The next subsection explains the concept of detectability and the details on probabilistic detectability measurements for different HS classification based on MD.

2.1. Quantifying the probabilistic detectability

The first step in probabilistic diagnosis is to define a set of HSs. These HSs can be classified based on the training data that include historical operation/failure data. The correct detection rate of each health status is one of the criteria to appraise the probabilistic performance of the sensor network. The correct detection rate can be determined as a conditional probability that the sensor network detects the same HS in which the system is operating at [15,25]. These correct detection rates will constitute the probability-of-detection (PoD) matrix, from which the detectability of each HS can be obtain for the sensor network.

2.1.1. Probability-of-detection (PoD) matrix

A PoD matrix defines the probability of the correct detection for each predefined HS. The general form of PoD matrix can be shown as:

$$\mathrm{PoD} = \begin{bmatrix} P_{11} & P_{12} & \cdots & P_{1N_{HS}} \\ P_{21} & P_{22} & \cdots & P_{2N_{HS}} \\ \vdots & \vdots & \ddots & \vdots \\ P_{N_{HS}1} & P_{N_{HS}2} & \cdots & P_{N_{HS}N_{HS}} \end{bmatrix} \tag{1}$$

where N_{HS} indicates the total number of classified HSs. P_{ij} is the probability that the system is detected as HS_j by the sensing system given that the system operates at HS_i. In the statistical form P_{ij} can be expressed as:

$$P_{ij} = \Pr\left(Detected\ as\ HS_j | Operated\ as\ HS_i\right) \tag{2}$$

Since any set of data from HS_i will be classified into one of the predefined N_{HS} health status, the summation of P_{ij} for $j = 1$ to N_{HS} is equal to unity, or $\sum_{j=1}^{N_{HS}} P_{ij} = 1$. In the PoD matrix, the diagonal terms (P_{ii}) will be defined as the detectability (D_i) that determines the probability of correct detection for each predefined HS, or

$$D_i = P_{ii} = \Pr(Detected\ as\ HS_i || opereted\ as\ HS_i) \tag{3}$$

In order to design a reliable sensor network, the detectability measured for each HS needs to satisfy the detectability target.

The following example explains the detectability measurements. One sensor is used to detect three different HSs. The first HS (HS_1) indicates there is no damage and the sensor data follows a normal distribution as $N(1, 0.8^2)$. The second HS (HS_2) represents some minor damage in the structure and the sensor data follows $N(4, 0.6^2)$. The third HS (HS_3) corresponds to severe damage and the sensor data follows $N(7, 1.4^2)$. Fig. 1 exhibits the PDFs for different HS in this example. Two neutral points (X_{1-2} and X_{2-3}) can be located where the normalized distances from different distributions are the same, or:

$$\frac{X_{1-2} - 1}{0.8} = \frac{4 - X_{1-2}}{0.6}, \quad X_{1-2} = 2.7142 \tag{4}$$

$$\frac{X_{2-3} - 4}{0.6} = \frac{7 - X_{2-3}}{1.4}, \quad X_{2-3} = 4.9000 \tag{5}$$

To obtain the detectability value for each HS we need to classify the sensory data into one of the three HS categories. The classification can be done by evaluating the normalized distances between the testing data and sensor output distribution for

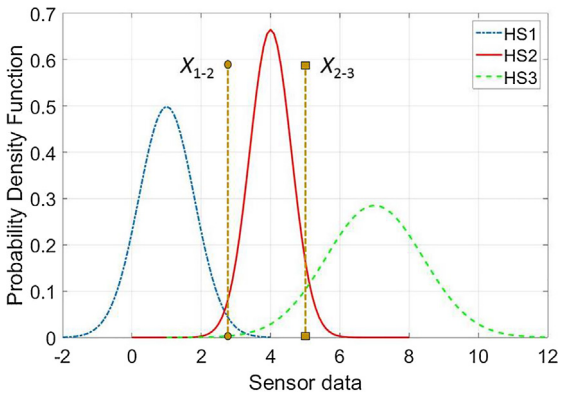

Fig. 1. Sensor output distribution or different HSs.

each HS. That is, the testing data are classified into each HS of which the normalized distance is smallest. In this one sensor example, this classification can be interpreted as integration of each PDF bounded by the neutral points as shown in Fig. 2, or:

$$D_1 = P_{11} = \Pr(Detected\ as\ HS_1 | Operated\ as\ HS_1) = \Pr\left(X \le X_{1-2} | X \sim N\left(1,\ 0.8^2\right)\right) = 0.9831 \tag{6}$$

$$D_2 = P_{22} = \Pr(Detected\ as\ HS_2 | Operated\ as\ HS_2) = \Pr\left(X_{1-2} \le X \le X_{2-3} | X \sim N\left(4,\ 0.6^2\right)\right) = 0.8959 \tag{7}$$

$$D_3 = P_{33} = \Pr(Detected\ as\ HS_3 | Operated\ as\ HS_3) = \Pr\left(X \ge X_{2-3} | X \sim N\left(7,\ 1.4^2\right)\right) = 0.9331 \tag{8}$$

In many engineering applications a sensor network is composed of numerous sensors and HSs where analytical evaluation of detectability is challenging. Therefore, more complex HS classification methods such as Mahalanobis Distance [26,27], linear discriminant analysis [28] or support vector machine [29] is required. Wang et al. [25] developed a detectability analysis approach using MD. This method is used due to its capability for classification of large amount of multivariate data specially when there is concern of affinities between groups. Next section briefly explains MD hired for classification of the random sensory signals.

2.2. Mahalanobis Distance (MD) classifier

Mahalanobis Distance (MD) measures the distance between online data points and the distribution of the training data sets, and it represents the similarities between the testing data and different training data sets – shorter distance represents greater similarities. That is, a testing data point can be categorized into a HS of which the MD is minimal. To compute MD, first we need to obtain the variance-covariance matrix $\mathbf{C}_x$ for the training data as:

$$\mathbf{C}_x = \frac{1}{(n-1)}(\mathbf{X} - \overline{\mathbf{X}})^T(\mathbf{X} - \overline{\mathbf{X}}) \tag{9}$$

where $\mathbf{X}$ is the training data matrix containing n objects in the rows measured for p variables, and $\overline{\mathbf{X}}$ is the matrix of variable means. Consequently, MD can be calculated as:

$$\mathrm{MD}_i = \sqrt{(x_i - \overline{x})\mathrm{C}_x^{-1}(x_i - \overline{x})^T} \tag{10}$$

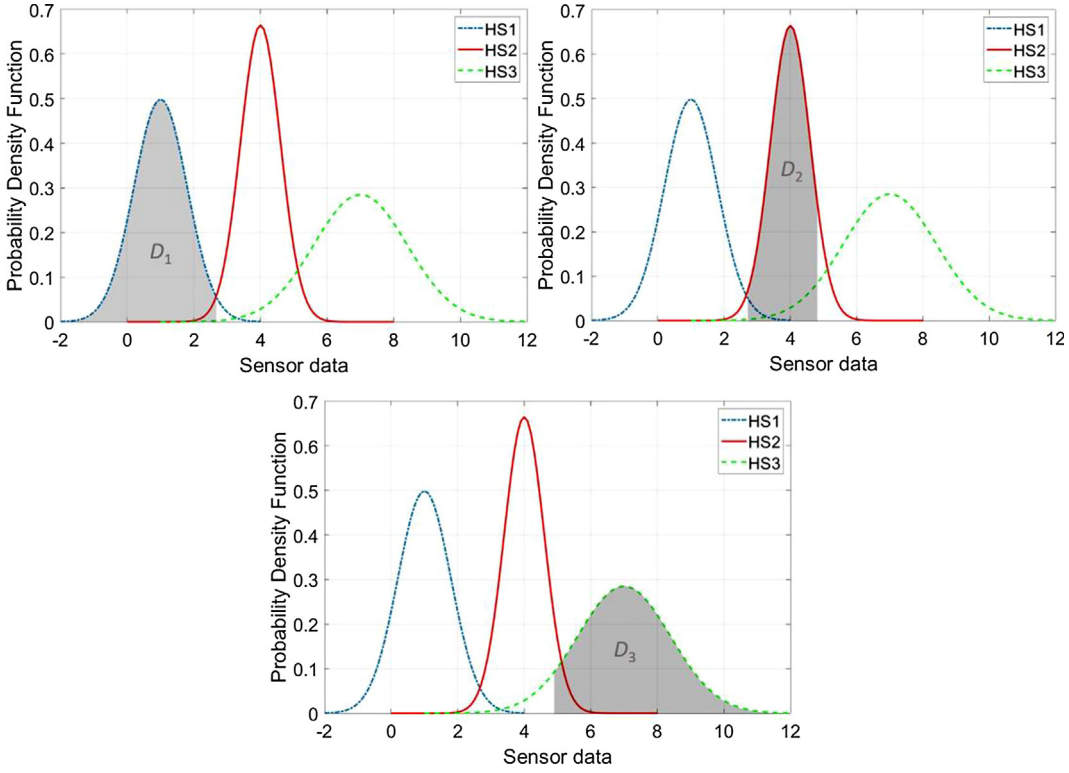

Fig. 2. Evaluated detectability for each HS.

where x_i is a testing data point to be classified and $\bar{x}$ is the mean of the training data. MD classifier categorizes the testing data sets obtained by a sensing system into a predefined HS.

Consider another example with two sensors and three predefined HSs. The training data for each sensor (Table 1) consists of a normally distributed random data for different HSs (1000 sensory data point for each HS). Six different testing data in the first two columns of Table 2 will be classified in one of the HSs, by evaluating MD in Eq. (10). The distribution of the training data for three different HS is shown in Fig. 3. At each HS, the MD is obtained for the testing data shown in Table 2. As discussed before, the testing data is classified into a group with the least MD. For instance, to classify the first testing data [3.02 1.45], three different MD values are measured using Eq. (1) to evaluate similarity to each group of training data in Table 1. Based on the MD values for HS_1, HS_2, and HS_3 (3.13, 2.96, and 4.02), one can classify this testing data to HS_2 because of the shortest MD.

3. Kriging for surrogate molding of the sensing network

One of the critical burdens in probabilistic sensing system design is the computational costs for evaluating stress, strain, or the corresponding sensor signals, especially when FEA is involved. Kriging is used in this paper that enables the assessment of sensor network with only a few number of simulation runs.

3.1. Overview of kriging

Kriging is a stochastic interpolation algorithm that has been used in many engineering simulation and optimization problems [30–34]. Basically, kriging is a generalized regression model which accounts for the correlation in the residual between the regression model and observation. Kriging constructs a trend function based on the sample data set and a Gaussian process using the residuals $Z(\mathbf{X})$. Assuming that the trend function is a linear combination of basis function the true response function takes the following form:

Table 1
Training data for each health status.

Health status	Sensor A	Sensor B
HS_1	$N(1.1,0.6^2)$	$N(1.5,0.4^2)$
HS_2	$N(1.7,0.5^2)$	$N(2.4,0.7^2)$
HS_3	$N(3.2,1.2^2)$	$N(5.1,0.9^2)$

Table 2
Health status classification using MD.

	Testing data		Mahalanobis Distance			Classified HS
	S_A	S_B	HS_1	HS_2	HS_3	
T1	3.02	1.45	3.13	2.96	4.02	HS_2
T2	6.70	3.79	10.73	9.85	3.18	HS_3
T3	0.05	2.06	2.32	3.28	4.21	HS_1
T4	2.01	3.56	11.08	7.27	9.44	HS_2
T5	−1.45	−0.52	6.54	7.41	7.16	HS_1
T6	2.08	0.79	2.44	2.48	5.01	HS_1

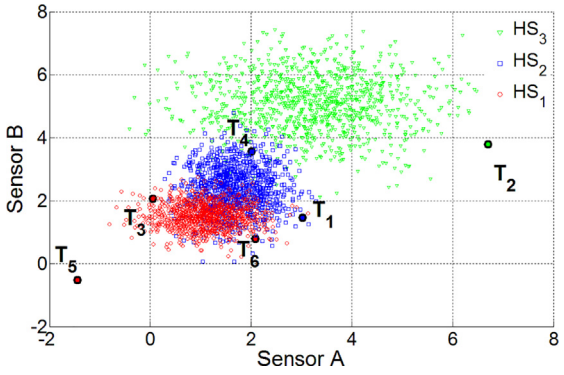

Fig. 3. Health status classification using MD.

$$\widehat{y}(\mathbf{X}) = \beta^T f(\mathbf{X}) + Z(\mathbf{X}) = \sum_{j=1}^{k} \beta_j f_j(\mathbf{X}) + Z(\mathbf{X}) \tag{11}$$

$\boldsymbol{\beta}^T\mathbf{f}(\mathbf{X})$ is the mean of the Gaussian process defined as the product between the regression coefficient β_j, and the basis function f_j, $j = 1, 2, \ldots, k$. $Z(\mathbf{X})$ is the residual composed of Gaussian and stationary random process with zero mean and covariance V:

$$V(x_1, x_2) = \sigma^2 \boldsymbol{R}(x_1, x_2) \tag{12}$$

where σ^2 is the process variance determined in the following of this section and $\boldsymbol{R}(x_1, x_2)$ is the correlation function. This function controls the smoothness of the model, the differentiability of the surface by quantifying the correlation between two observations, and the influence of nearby points. In this study Gaussian function has been utilized and defined with only one parameter $\theta > 0$ which controls the range of influence of nearby points [35].

$$\boldsymbol{R}(x_1 - x_2) = \exp\left[-\theta |x_2 - x_1|^2\right] \tag{13}$$

Considering the sampled design variable vector $\mathbf{X} = \{x_1, x_2, \ldots, x_n\}$ as a subset of the input variable domain Ω and the corresponding output results as $\mathbf{Y} = \{y_1, y_2, \ldots, y_n\}$, the linear predictor of the output has the form of:

$$\widehat{y}(x) = \lambda^T(x)\mathbf{Y} \tag{14}$$

At any arbitrary point kriging approximation treats $\widehat{y}(x)$ as a random function, which tries to minimize the mean square error (MSE) in order to find the best linear unbiased predictor. The MSE can be evaluated as:

$$\mathrm{MSE}\left[\widehat{y}(x)\right] = E\left[\lambda^T(x) - y(x)\right]^2 \tag{15}$$

subject to unbiased constraint:

$$E\left[\lambda^T(x)\mathbf{Y} - y(x)\right] = 0 \tag{16}$$

Universal kriging is a general form of kriging that determines a set of regression functions as $f(x) = \{f_1(x), f_2(x), \ldots, f_k(x)\}^T$. A quadratic form of regression model (second order polynomial) has been used in this paper. Eq. (17) represents this function.

$$\begin{aligned} &f_1(x) = 1, \\ &f_2(x) = x_1, \ \ldots, f_{n+1}(x) = x_n, \\ &f_{n+2}(x) = x_1^2, \ \ldots, f_{2n+1}(x) = x_1 x_n, \\ &f_{2n+2}(x) = x_2^2, \ \ldots, f_{3n}(x) = x_2 x_n, \\ &\ldots, f_k(x) = x_n^2 \\ &k = \tfrac{1}{2}(n+1)(n+2) \end{aligned} \tag{17}$$

Among these, n functions are chosen for linear combination of $f_i'(x)$ to minimize the MSE in Eq. (15). Then the generic information matrix $\mathbf{F}$ can be obtained by evaluating first order derivatives at each n observation points as:

$$\mathbf{F} = \begin{bmatrix} f_1'(x) \\ f_2'(x) \\ \vdots \\ f_n'(x) \end{bmatrix} \tag{18}$$

Eq. (19) indicates the correlation matrix which is constructed by correlation functions at each possible combination of observation points.

$$\mathbf{R} = \begin{bmatrix} \boldsymbol{R}(x_1, x_1) & \boldsymbol{R}(x_1, x_2) & \cdots & \boldsymbol{R}(x_1, x_n) \\ \boldsymbol{R}(x_2, x_1) & \boldsymbol{R}(x_2, x_2) & \cdots & \boldsymbol{R}(x_2, x_n) \\ \vdots & \vdots & \ddots & \vdots \\ \boldsymbol{R}(x_n, x_1) & \boldsymbol{R}(x_n, x_2) & \cdots & \boldsymbol{R}(x_n, x_n) \end{bmatrix} \tag{19}$$

$\mathbf{R}$ is a positive semidefinite and symmetric matrix where the diagonal terms are all equal to one. To estimate the $\widehat{y}(x)$ in Eq. (14) we need to define $\mathbf{r}(x)$ which represents the correlation between an unknown point and the n known samples:

$$\mathbf{r}(x) = \{\boldsymbol{R}(x, x_1), \boldsymbol{R}(x, x_2), \ldots, \boldsymbol{R}(x, x_n)\}^T \tag{20}$$

Considering that $\lambda(x)$ is found to minimize MSE in Eq. (15) subject to the constraint mentioned in Eq. (16), $\widehat{y}(x)$ known as best linear unbiased predictor (BLUP) would be obtained by:

$$\widehat{y}(x) = f'^{T}(x)\,\widehat{\beta} + r^{T}(x)\mathbf{R}^{-1}\left(\mathbf{Y} - \mathbf{F}\,\widehat{\beta}\right) \tag{21}$$

and the least-squares estimation of $\widehat{\beta}$ would be:

$$\widehat{\beta} = \left(\mathbf{F}^{T}\mathbf{R}^{-1}\mathbf{F}\right)^{-1}\mathbf{F}^{T}\mathbf{R}^{-1}\mathbf{Y} \tag{22}$$

Knowing this term, the process variance can be expressed as $\sigma^2 = (1/n)\left(\mathbf{Y} - \mathbf{F}\,\widehat{\beta}\right)^{T}\mathbf{R}^{-1}\left(\mathbf{Y} - \mathbf{F}\,\widehat{\beta}\right)$. Consequently, the predicted response function $\widehat{y}(x)$ at a new point x has a joint Gaussian distribution with the mean and variance as follows:

$$\begin{aligned}\mu_{\widehat{y}}(x) &= f'(x)^{T}\beta + \mathbf{r}(x)^{T}\mathbf{R}^{-1}(\mathbf{Y} - \mathbf{F}\beta)\\ \sigma^2_{\widehat{y}}(x) &= \sigma^2\left(1 - \mathbf{r}(x)^{T}\mathbf{R}^{-1}\mathbf{r}(x) + u^{T}(x)\left(\mathbf{F}^{T}\mathbf{R}^{-1}\mathbf{F}\right)^{-1}u(x)\right)\end{aligned} \tag{23}$$

where $u(x) = \mathbf{F}^{T}\mathbf{R}^{-1}\mathbf{r}(x) - f'(x)$. The first term in Eq. (21) represents the generalized least-squares estimation of a random point $x \in \Omega$ given the correlation matrix $\mathbf{R}$. The second part pulls the generalized least-squares estimation via the observation points. The MSE is zero at the observation points since there is no uncertainty. As $\boldsymbol{x}$ moves away from observation points, however, the uncertainty becomes larger and it results in the second component in Eq. (21) approaches to zero and the MSE becomes closer to the process variance σ^2. More details on kriging can be found at Ref. [36,37]. Selection of sample points for the kriging model is very important to reduce the statistical uncertainty of the predicted model. Latin hypercube sampling (LHS), initially proposed in Ref. [38], is used as the sampling scheme in this paper for the metamodel based optimization. LHS is a stratified sampling strategy for generating random samples which ensures all portions of the design space is covered. Consider sampling m points in an n dimensional vector space, the LHS divides each dimension into m intervals with equal probability and without any overlapping. Since we consider a uniform distribution for design variables, the intervals have equal sizes. A single point is chosen from each interval per each dimension, and to make combination from each dimension to complete pairing.

4. General RBDO formulation

Reliability-based design optimization (RBDO) finds the optimum design of an engineered system that minimizes the design cost and satisfies the reliability target with respect to system constraints, while accounting for various sources of uncertainty [39–41]. In general, the RBDO problem can be formulated as follows:

$$\begin{aligned}&\text{Minimize } f(\mathbf{d})\\ &\text{Subject to } R_i = \Pr(G_i(\mathbf{x},\theta;\mathbf{d}) \le 0) \ge \Phi(\beta_i^t) = R_i^t, \quad i = 1,\ldots,N_c\\ &d_j^L \le d_j \le d_j^U, \quad j = 1,\ldots,N_d\end{aligned} \tag{24}$$

where f is the objective function, $\mathbf{x} = [x_1, \ldots, x_{Nd}]^{\mathrm{T}}$ is the vector of random design variables, $\boldsymbol{\theta} = [\theta_1, \ldots, \theta_{Nr}]^{\mathrm{T}}$ represents the random parameter vector with N_d and N_r being the numbers of random design variable and random parameters, respectively. $\mathbf{d} = [d_1, \ldots, d_{Nd}]^{\mathrm{T}} = \boldsymbol{\mu}(\mathbf{x})$ is the mean design vector (or the design variable set), R_i is the reliability level of the ith design constraint for a given system design $\mathbf{d}$, G_i is the ith design constraint for $i = 1, \ldots, N_c$ when N_c is the number of constraints, $\Phi(\cdot)$ is the cumulative distribution function of the standard normal distribution, R_i^t is the target reliability level of the ith constraint corresponding to the target reliability index β_i^t, and d_j^L and d_j^U are the lower and upper bounds for the design variable vector, respectively.

4.1. Proposed detectability measurements in RBDO framework

The detectability measurements in the optimization process is proposed in 4 steps.

- Step 1 – Data sample formation: Generate input data in the domain of design variables, obtain the sensor outputs, and categorize them into different HS conditions. In this step direct simulation (e.g. FEA) is done to obtain sensory data.
- Step 2 – Surrogate model construction for obtaining the stochastic sensory signal: Based on the simulated data in Step 1, LHC picks the sample points to construct a kriging model by Eq. (21). At this point, the model is ready to estimate the desired output for any arbitrary point.
- Step 3 – Estimation of the stochastic sensory signal: Generate random samples based on the desired sensor locations. The sensor output signal is estimated for the desired sensor patches using the constructed kriging model (training/testing data).
- Step 4 – Statistical evaluation of detectability: Calculate the detectability for different HSs using the training and testing data as described in Section 2.1.1.

The genetic algorithm (GA) is used as the optimization tool to find the optimum solution in the RBDO problem in Eq. (24). GA is superior to gradient descent techniques since the search is not biased towards local optima. RBDO starts with the initial random guess selected by GA optimizer and will minimize the cost function subject to detectability constraints. This overall procedure is explained in Fig. 4.

5. Case study: joint failure in a skin panel

Rivet joint is one of the popular methods to assemble skin (or panel) structures in many engineering applications such as aerospace structures, civil infrastructures, and vehicles. SHM for such systems is highly required because varied environmental condition (humidity, temperature) as well as operational conditions (pressure, speed, and loading condition) cause multiple types of structural damages such as corrosion, delamination, cracks, detachment. In this section we develop reliability based design optimization (RBDO) for the smart sensing network capable of failure diagnosis in skin structures. Fig. 5 depicts the configuration of the rectangular aluminum panel (40 cm $\times$ 30 cm $\times$ 1.15 mm) used in this example with the rivet joints indexed as J_1–J_8. The density and yield stress for the plate are 2.73 g/cm^3 and 125 MPa, respectively. A harmonic force F = 2.5 N with a frequency of 17 Hz is applied at the center of the panel. The goal is to design a PZT sensor network to minimize the volume of PZT material (shown by green squares in Fig. 5) subject to the constraints on detectability (i.e. probability of detection for the rivet joint failure). Eight different HSs are considered for this panel based on the damage combination of three joints (J_4, J_6, J_7) as shown in Table 3. Two particular health status are shown in Fig. 6: HS_0 and HS_7, respectively.

In the following sections we will explain the FEA model used to appraise the performance of sensing network for the proposed algorithm and how the RBDO improves the reliability of sensor network.

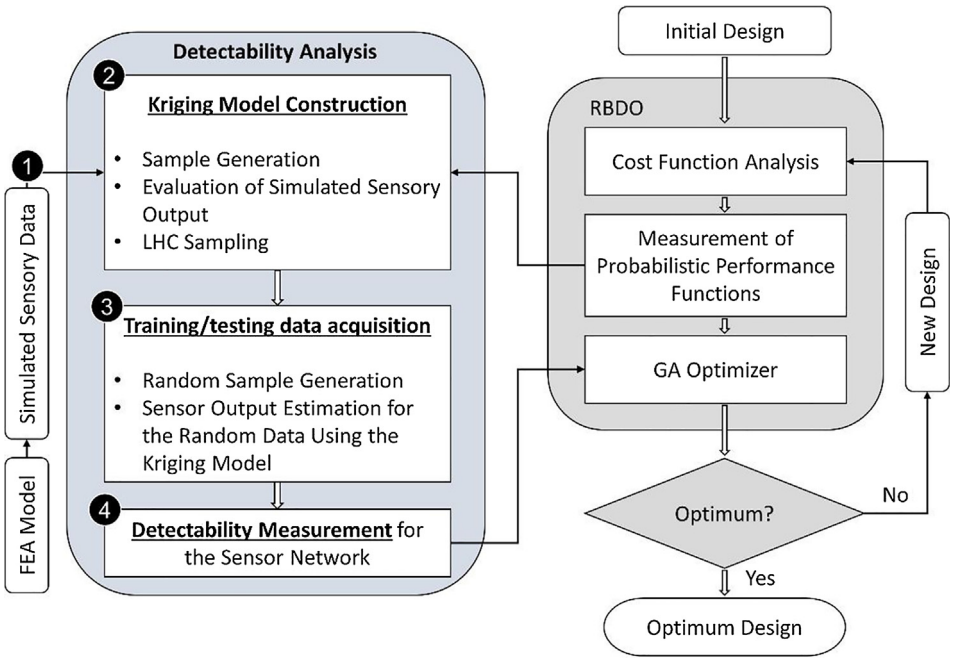

Fig. 4. RBDO flowchart for sensing network design.

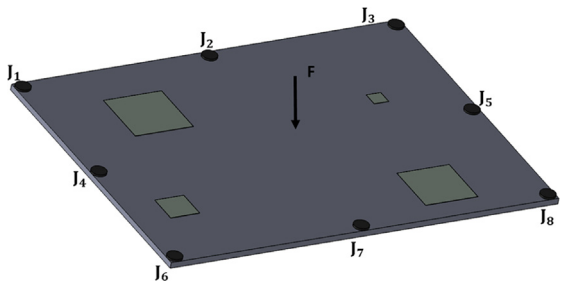

Fig. 5. Configuration of the skin structure with the attached rivet joints.

Table 3
Demonstration of different HS categories.

Health status	HS_0	HS_1	HS_2	HS_3	HS_4	HS_5	HS_6	HS_7
Damaged joint	None	J_6	J_7	J_4	J_6, J_7	J_6, J_4	J_4, J_7	J_4, J_6, J_7

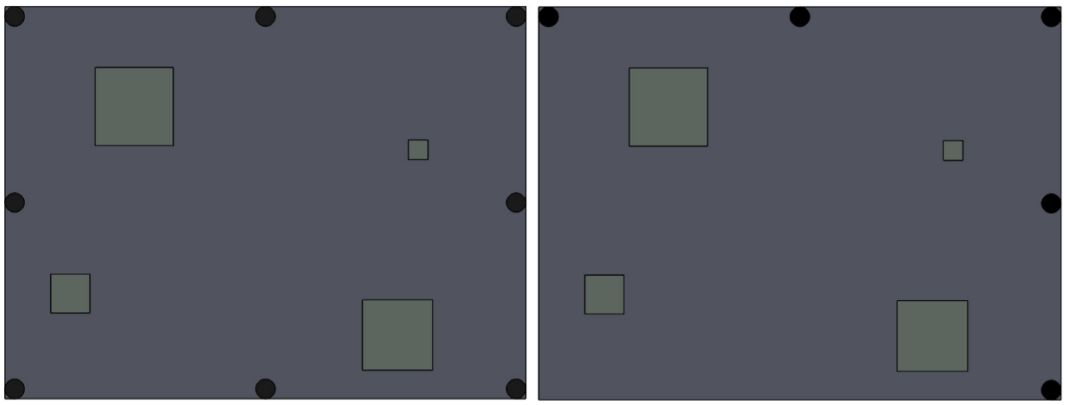

Fig. 6. Boundary conditions to reflect different HS (a) HS_0, (b) HS_7.

5.1. FEA model

For generation of the training data, a finite element analysis model is developed in ANSYS which directly measures the voltage outputs from multiple sensors for a given configuration of sensor patch as well as the health condition of the joints defined in Table 3. In the FEA model, 3-D elements including SOLID186 and SOLID226 are used to represent the skin panel and PZT material respectively. Element CIRCU94 is connected to each PZT sensor to measure the generated voltage output. In total the model consists of 15,037 3-D elements and 22,851 nodes. Each HS is represented by different boundary conditions (BC) – fixed BC for healthy rivet joint and no BC for damaged/detached rivet joint. Harmonic analysis is used to appraise the performance of the sensor network.

The location and size of the sensor patches determines the electrical output response for a given failure mode. Fig. 7(a) and (b) depict the output voltage of the patches at HS_0 and HS_7 respectively for the different sensor size and location. It can be observed that the signals are affected by the size and location of sensors as well as the HS. The purpose of this sensor network is to distinct the sensory data from different HSs with minimum use of the PZT patches. Realistic operating condition involves uncertainty such as loading condition, geometrical parameters, and material properties, and the corresponding sensory signal output has uncertainty as well. This is why reliability-based design optimization is used to consider the uncertainty of the system in the design process. The next section explains the corresponding RBDO formulation.

5.2. Reliability-based design optimization formulation

RBDO aims to find the best compromise between the cost function and probabilistic constraints. In this problem the cost function is to minimize the total area (or volume) of the sensor patches. The sensing system needs to satisfy the detectability target for each HS. The RBDO formulation can be written as:

$$\begin{aligned} &\textit{Minimize} && \textstyle\sum_{j=1}^{N} A_j \\ &\textit{subject to}: && D_i(\mathbf{x}, \boldsymbol{\theta}; \mathbf{d}) \geq D_T \\ & && \mathbf{x}^L \leq \mathbf{x} \leq \mathbf{x}^U \\ & && \mathbf{d}^L \leq \mathbf{d} \leq \mathbf{d}^U \end{aligned} \tag{25}$$

where the objective function A_j represents the PZT area for each square patch of sensor and N is the number of sensors that could vary from 1 to 4. D_i is the detectability in Eq. (3) and its target value D_T is set to be 99.5%. In this case study we considered three random parameters ($\boldsymbol{\theta}$) including the overall length and width of the skin panel, and the amplitude of harmonic force applied to the center of the plate. The deterministic design variable set ($\mathbf{d}$) comprises the side length of each squared PZT patch and the location of the sensor – the X-Y coordinates of the left-bottom corner. In total there are 3 random parameters and 3 $\times$ N number of design variables as depicted in Tables 4 and 5, respectively.

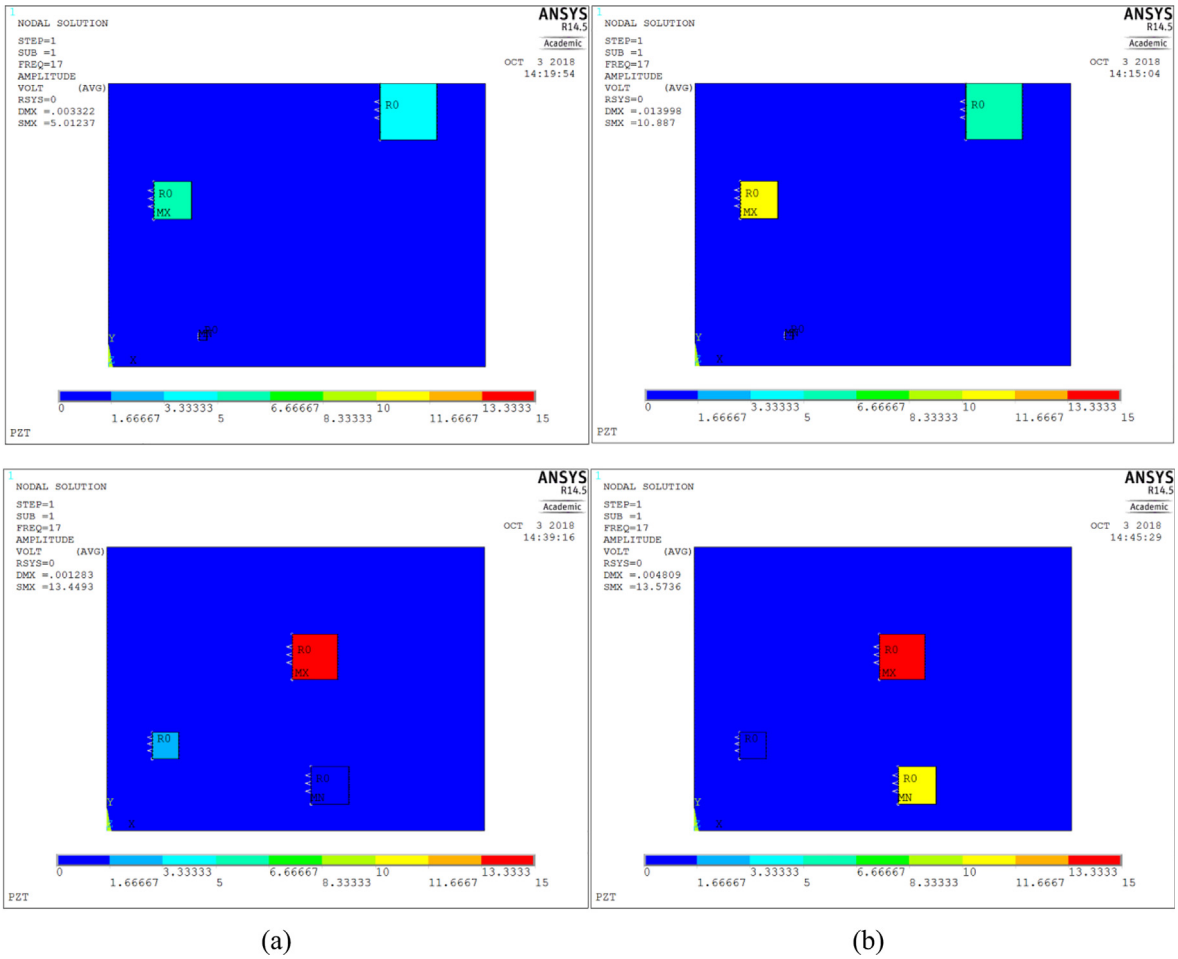

Fig. 7. Voltage contours for different size and location of sensor patches (a) HS_0, (b) HS_7.

Table 4
Random parameters for the sensor network design.

Random parameter	Description	Distribution type	Mean	Standard deviation
θ_1 (cm)	Length of skin panel	Normal	40	0.4
θ_2 (cm)	Width of skin panel	Normal	30	0.3
θ_3 (N)	Amplitude of the harmonic force	Normal	2.5	0.025

Table 5
Deterministic design variables for the sensor network design.

Variable	Description	Lower bound	Upper bound
X_j (cm)	X coordinate of the jth sensor patch	0	34
Y_j (cm)	Y coordinate of the jth sensor patch	0	24
S_j (cm)	Side length of the jth sensor patch	2	6

The stepwise process in Section 4.1 is done for detectability calculation in RBDO. In Step 1, random sample points (900 samples) are generated on the design variables (Table 4), the random parameters (Table 5), HSs (Table 3), and the corresponding sensor output voltage. In Step 2, the data set in Step 1 is used to construct a kriging model that describes the sensor output voltage as a function of the HS and the design variables (i.e., sensor locations and sizes). Step 3 uses the kriging model in Step 2 to generate two data sets (training data and testing data, 800 data point for each). This step considers the geometrical random parameters (Table 4) to obtain the vibrational pattern of the skin panel at each HS, and the vibration pattern is

used as input parameter to the kriging model to obtain the sensor output voltage. In Step, 4 MD classifier and the detectability measures at each HS are figured out from these two data sets.

5.3. Simulation results

This section presents the results of the skin panel sensor network design problem formulated in Section 5.2. The ultimate goal of RBDO in this sensor network design is to find the best arrangement for the minimum number of sensors with the highest failure detectability. At each health status, detectability can be obtained as a function of sensor location represented by its ordinates (X, Y) and size of the sensor (S). The Genetic algorithm (GA) iteratively updates the sensor locations and sizes to meet the detectability target while minimizing the PZT material use. The optimization process is conducted for different number of sensors from $N = 1$ to $N = 4$. When the number of sensors is one or two ($N = 1$ or 2), the algorithm could not find a design that satisfies the detectability target. The optimum solution is obtained for three sensor patches ($N = 3$) after 23 iterations with the detectability target satisfied. The GA iteration history on the design variables $\mathbf{d}$ is shown in Table 6. Table 7 depicts the history on detectability and cost function, where one can confirm the detectability values have reached the target for all different HSs. This detectability change can be reviewed graphically in Fig. 8(a). Throughout this optimization, the total area of the sensor patches has reduced down from 71.36 to 37.44 cm^2 (Fig. 8(b)).

Fig. 9 depicts the location/size of three PZT patches for the optimum results (detectability = 99.5%). In the next section we investigate the performance of these two systems for the failure detection of rivet joints.

5.4. Experimental verification of the results

The failure detectability of the sensor network in Section 5.3 is experimentally evaluated. Fig. 10 shows the experimental setup used in this study, composed of: shaker (ET-126B, Labworks Inc), function generator (AFG3022C, Tektronix), and oscilloscope (DSO5202P-INTERNATIONAL, Hantek). The aluminum panel is coated with paint to minimize electrical interaction with the sensors. The rivet joint is represented using bolts due to their convenience on health status change (by fastening/loosening). The eight rods supporting the plate are mounted on the optical table with the brackets. A tightly fastened bolt indicates the healthy condition of the joint and a loosened one represents the failure of the corresponding joint. The panel is excited by the electrodynamic shaker on the center of the plate. Function generator generates the electrical waveform for the harmonic excitation (2.5 N harmonic force at 17 Hz). The output voltage of each sensor patch is obtained using the oscilloscope. To further explain the effectiveness of the proposed method, another configuration of sensor location is considered with average detectability of 50%. Fig. 11 depicts the location/size of three PZT patches for this case.

The experiment has been done for two different cases: Case I – the optimum RBDO result in Section 4 (detectability 99.5%), and Case II – a separate RBDO result with lower detectability target (50.0%). In the experiment, eight different HSs are realized by loosening the corresponding bolts in Table 3 and the output signal is measured from each sensor. Due to the uncertainties involved in the sensing system and measurement process, the output signal of each sensor has uncertainty as well. The output sensory signals for the two cases are measured to obtain the experimental detectability level for each

Table 6
Iterative history of RBDO for the skin panel example (all numbers in cm).

Iter	X_1	Y_1	S_1	X_2	Y_2	S_2	X_3	Y_3	S_3
1	23.2	20	2	19.6	7.2	5.6	0	16	6
2	23.2	19.6	2.4	19.6	6.8	5.2	0	16	6
3	6	0.8	2.8	16.4	0.8	5.2	4.8	10.4	5.6
4	7.6	13.6	4.4	14.8	0.4	5.2	18	10.4	3.6
5	4	10.8	5.6	15.6	0	3.6	16.8	10	3.2
6	18.8	18.8	4	17.2	0.8	4.8	0	14.8	3.6
7	19.6	18.8	4	17.6	0.8	4.4	0	15.6	3.6
8	20	19.2	4	17.2	0.8	4.4	0	15.2	3.2
9	20	19.2	3.6	17.6	0.8	4.4	0	15.6	3.2
10	20	18.8	3.6	18	0.4	4	0	15.6	3.2
11	20	19.2	3.2	17.6	0.8	4.4	0	15.6	2.8
12	19.6	14.8	3.6	16.8	0.4	4	0	15.6	2.8
13	20	19.2	2.8	17.6	0.8	4.4	0	16	2.8
14	20	19.2	2.4	17.6	0.8	4.4	0	15.6	2.8
15	20.4	19.2	2.8	17.6	0.4	4	0	15.6	2.8
16	20.4	17.2	2	17.2	0.8	4	0	16	2.8
17	20.4	19.2	2.8	17.2	0.4	3.6	0	15.6	2.4
18	20.4	19.2	2.4	17.6	0.4	3.6	0	16	2
19	20.4	20	2	16	0.4	3.2	0	15.6	2.8
20	20.4	19.2	2.4	17.2	2.4	3.2	0	15.6	2
21	20.8	19.2	2	17.2	2.8	3.2	0	15.6	2
22	20.8	19.2	2	17.2	2.4	2.8	0	15.6	2
23	20.8	18.8	2	16.8	4	2.4	0	15.6	2

Table 7
Detectability and cost function of RBRD for skin panel example.

Iter	D_0	D_1	D_2	D_3	D_4	D_5	D_6	D_7	Cost function (cm^2)
1	0.850	0.785	0.880	0.847	0.761	0.856	0.902	0.864	71.36
2	0.857	0.807	0.885	0.863	0.763	0.869	0.903	0.866	68.8
3	0.880	0.832	0.898	0.867	0.777	0.886	0.905	0.875	66.24
4	0.882	0.854	0.899	0.871	0.810	0.892	0.910	0.891	59.36
5	0884	0.856	0.904	0.878	0.839	0.896	0.922	0.898	54.56
6	0.884	0.859	0.906	0.881	0.849	0.910	0.924	0.904	52.0
7	0.906	0.869	0.918	0.884	0.852	0.922	0.931	0.920	48.32
8	0.909	0.897	0.921	0.896	0.868	0.934	0.949	0.920	45.6
9	0.916	0.899	0.926	0.896	0.873	0.935	0.950	0.923	42.56
10	0.927	0.914	0.930	0.908	0.886	0.936	0.951	0.929	39.2
11	0.928	0.937	0.938	0.926	0.890	0.946	0.954	0.938	37.44
12	0.928	0.940	0.948	0.929	0.898	0.949	0.959	0.941	36.8
13	0.937	0.940	0.950	0.931	0.899	0.962	0.962	0.941	35.04
14	0.960	0.948	0.959	0.942	0.933	0.972	0.963	0.941	32.96
15	0.960	0.951	0.972	0.962	0.939	0.977	0.966	0.945	31.68
16	0.975	0.957	0.977	0.966	0.957	0.984	0.971	0.962	27.84
17	0.985	0.959	0.988	0.967	0.966	0.991	0.985	0.966	26.56
18	0.993	0.972	0.988	0.967	0.971	0.991	0.992	0.975	22.72
19	0.994	0.972	0.991	0.972	0.984	0.993	0.992	0.979	22.08
20	0.994	0.986	0.995	0.994	0.986	0.993	0.994	0.992	20.0
21	0.994	0.994	0.995	0.995	0.994	0.994	0.994	0.994	18.24
22	0.995	0.994	0.995	0.995	0.994	0.995	0.995	0.995	15.84
23	0.995	0.995	0.995	0.995	0.995	0.995	0.995	0.995	13.76

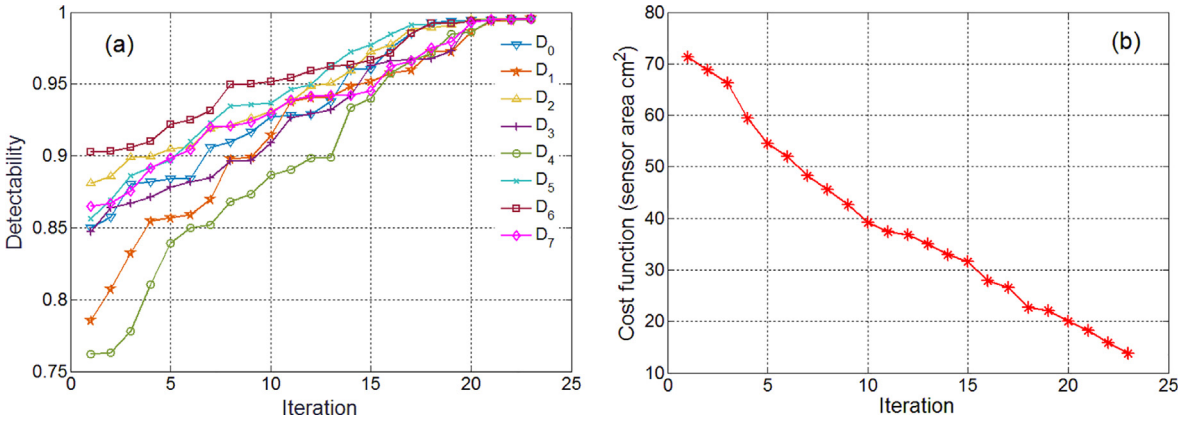

Fig. 8. RBDO iterative results in Table 7 (a) Detectability improvement; (b) Cost function.

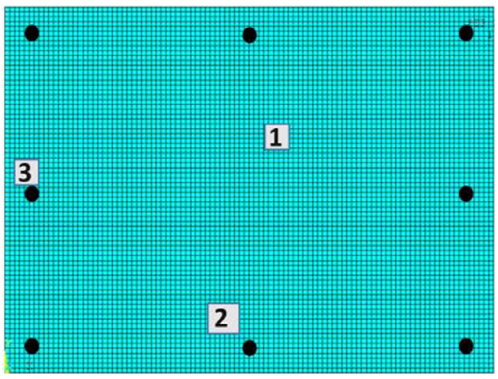

Fig. 9. Sensor configuration for Detectability = 99.5%.

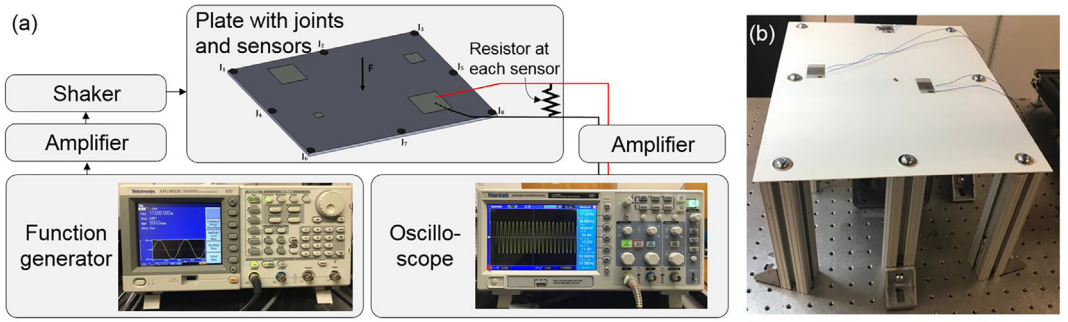

Fig. 10. Experimental setup: (a) device connection with the panel; (b) panel test setup with three sensors.

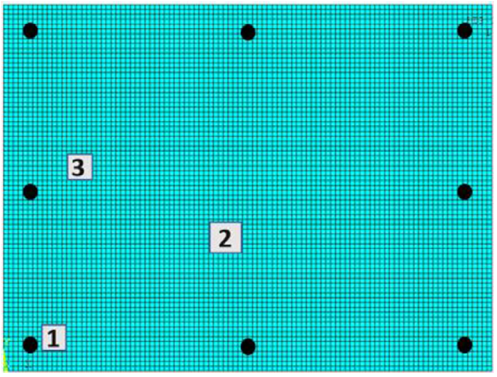

Fig. 11. Sensor configuration for Detectability = 50%.

Table 8
Sensor location and size for the experiments (cm).

	CaseI			CaseΠ		
	Coordinate of the left-bottom corner		Sensor side length	Coordinate of the left-bottom corner		Sensor side length
	x	*y*		*x*	*y*	
Sensor 1	20.8	18.8	2	3.2	2	2
Sensor 2	16.8	4	2.4	16.4	9.2	2.4
Sensor 3	0.8	15.6	2	4.8	16	2

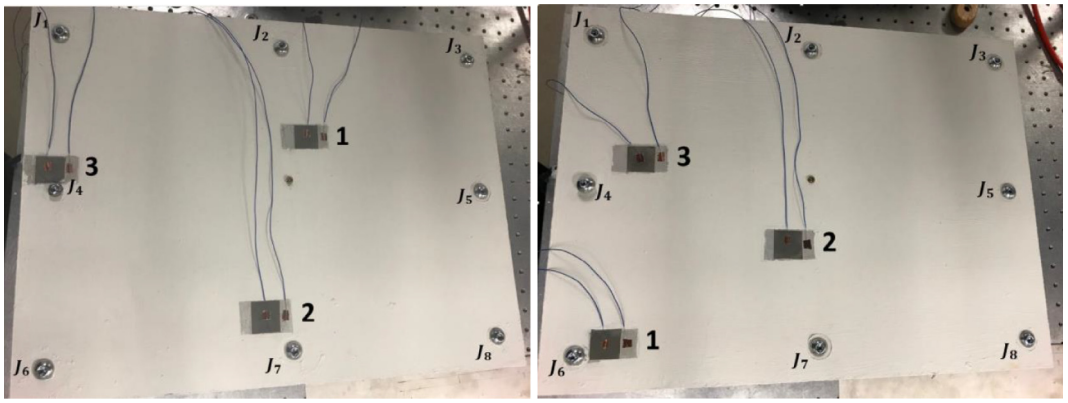

Fig. 12. Sensor placement in the experimental test for two different cases.

scenario and compare the effectiveness of algorithm for optimal placement of the sensors despite the presence of uncertainties. The sensor locations for the two different cases is shown in Table 8 and Fig. 12.

A number of the experimental data is recorded (1000 times of voltage measurement) at 8 different HSs (in total 8000 data) to investigate uncertainty. Table 9 shows the mean voltage value for each HS. Fig. 13 represents the distribution of the voltage for 1000 data points at each HS. For detectability measurement using Mahalanobis Distance (MD), both mean values and distribution (standard deviation) of the sensor output are taken into account. As a graphical representation, it can be observed that the distribution of the sensory data from Case I (Fig. 13(a)) is more distinct compared to Case II (Fig. 13(b)). It verifies that the MD measure can be used to detect the current operating HS with higher probability. These 1000 data points were used as the training data sets for extracting the damage features by measuring the amount of deviation from different HSs. 100 random data points were chosen separately at each HS as the testing data and MD were calculated between the training and testing data. Fig. 14 shows the probability density of the calculated MD for all 8 different HSs. Fig. 14(a) corresponds to Case I where target detectability is 99.5%. It can be observed that the MD corresponding to the current HS has the lowest mean value and its PDF is well separated from the other PDFs. The lowest mean indicates the least

Table 9
Mean values of the sensor voltage output.

Operating Health Status	Case I			Case II		
	Mean values of the peak voltage (Volt)					
	Sensor 1	Sensor 2	Sensor 3	Sensor 1	Sensor 2	Sensor 3
HS_0	1.76	3.49	1.16	10.33	13.56	1.44
HS_1	8.22	3.60	4.09	10.20	12.98	1.71
HS_2	19.52	3.06	2.76	9.62	9.43	2.25
HS_3	5.84	3.42	2.91	10.06	14.87	0.90
HS_4	4.66	6.41	4.5	8.76	10.87	2.01
HS_5	5.80	6.39	1.57	10.07	18.09	1.96
HS_6	26.64	5.10	4.26	9.04	10.98	4.67
HS_7	13.35	2.66	6.54	4.17	15.75	6.56

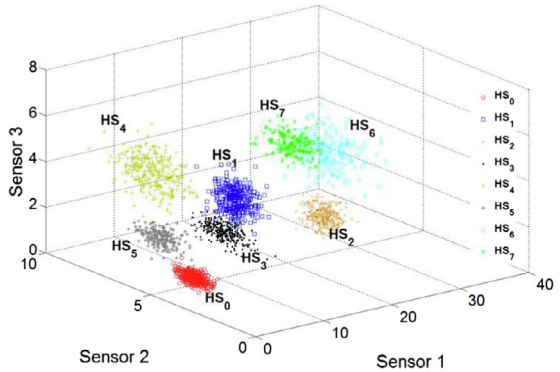

(a) Case I

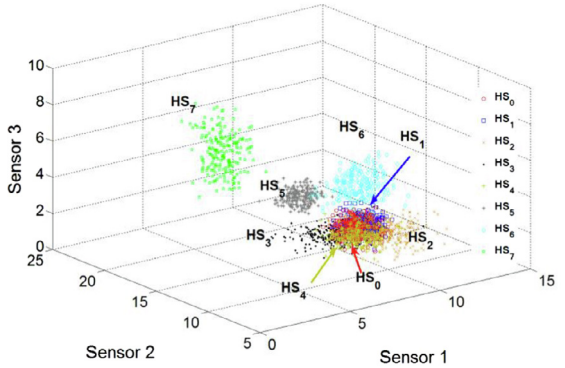

(b) Case II

Fig. 13. Peak voltage (Volts) distribution for different HSs.

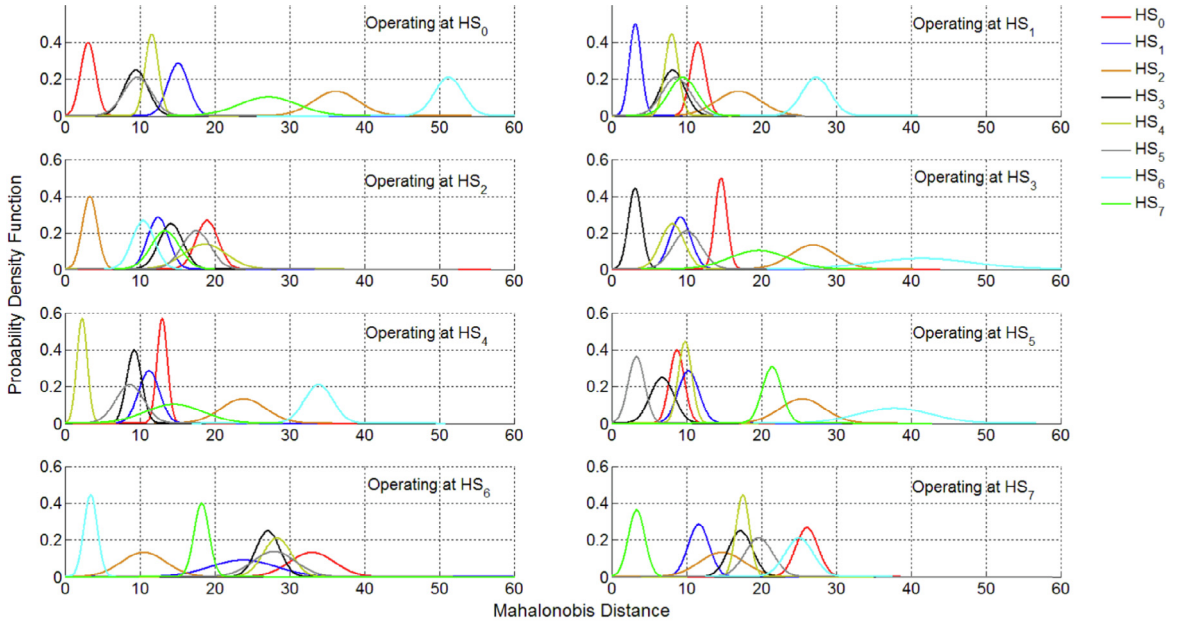

(a) Case I

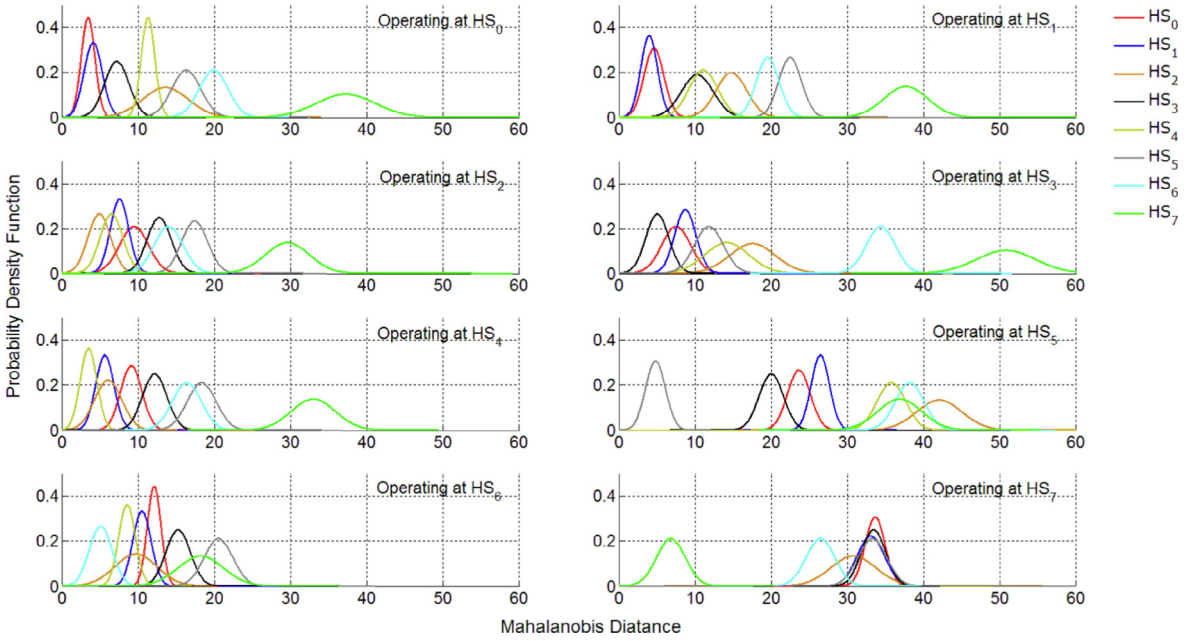

(b) Case Π

Fig. 14. Mahalanobis Distances for sensor network at different operating health status.

deviation between training and testing data which leads to detect the corresponding HS correctly. However, Case II experiment in Fig. 14(b) does not show well distinguished MD distributions between the HSs. For instance, when system is operating at HS_0, the PDF of MDs overlap between HS_0, HS_1, and HS_3 (red, blue, and black curves). This situation happens for most of the HSs in Case II. This indicates that the sensor configuration in Case II cannot determine the HS of the system with high accuracy. This study suggests that the proposed method can be successfully used to design the sensor network that identify different structural health status of a structure.

6. Conclusion

In this paper we presented a design method for the optimal placement of sensors in order to increase the probability of failure detection. Detectability measurements based on Mahalanobis Distance was used to define the essential number and location of the sensors in presence of uncertainty. Kriging method was used to build a surrogate model that estimates the probabilistic performance functions and minimize the computational burdens. A sample problem was discussed to demonstrate the capability of this method on detection of the joints damage in a skin panel using PZT sensors. The reliability-based design optimization problem was defined to find the optimal sensor network (size, location) that meets detectability requirement when load and geometrical uncertainty are considered. The experimental test was conducted for the optimum case (detectability = 99.5%) and the case with lower detectability (50%). The optimum result precisely detected the health status of the system based on the fact that the Mahalanobis Distance for the operating HS has the least mean value, and it is well separated from the other HSs. For the lower detectability case, the Mahalanobis Distance distributions has significant overlaps among multiple HSs. The results demonstrated versatility of the proposed method for the sensor network design with consideration of various uncertainty. The novelty of this method lies in the integration of training and testing data with a probabilistic sensing model using kriging, and its experimental verification for optimal sensor network design. Despite the fact that system could perform under several HSs and the large number of data to be analyzed, the proposed method could precisely diagnose the health condition. Future work includes extension of the current sensor design framework to random vibration input and appraise the capability of system failure detection.

Acknowledgment

The authors acknowledge Mr. Jason Pentsil on his assistance to piezoelectric sensor test.

References

[1] V. Gupta, M. Sharma, N. Thakur, Optimization criteria for optimal placement of piezoelectric sensors and actuators on a smart structure: a technical review, J. Intell. Mater. Syst. Struct. 21 (12) (2010) 1227–1243.
[2] A.-C. Lee, S.-T. Chen, Collocated sensor/actuator positioning and feedback design in the control of flexible structure system, ASME J. Vib. Acoust., 1994, pp. 146–154.
[3] H.W. Zhang, B. Lennox, P.R. Goulding, A.Y.T. Leung, A float-encoded genetic algorithm technique for integrated optimization of piezoelectric actuator and sensor placement and feedback gains, Smart Mater. Struct. 9 (4) (2000) 552–557.
[4] S. Leleu, H. Abou-Kandil, Y. Bonnassieux, Piezoelectric actuators and sensors location for active control of flexible structures, IEEE Trans. Instrum. Meas. 50 (6) (2001) 1577–1582.
[5] Y.D. Kim, J.L. Junkins, Measure of controllability for actuator placement, J. Guidance Control Dyn. 14 (5) (1991) 895–902.
[6] D. Halim, S.O.R. Moheimani, An optimization approach to optimal placement of collocated piezoelectric actuators and sensors on a thin plate, Mechatronics 13 (1) (2003) 27–47.
[7] E.B. Flynn, M.D. Todd, A Bayesian approach to optimal sensor placement for structural health monitoring with application to active sensing, Mech. Syst. Sig. Process. 24 (4) (2010) 891–903.
[8] Y.J. Cha, A.K. Agrawal, Y. Kim, A.M. Raich, Multi-objective genetic algorithms for cost-effective distributions of actuators and sensors in large structures, Expert Syst. Appl. 39 (9) (2012) 7822–7833.
[9] M. Sunar, S.S. Rao, Thermopiezoelectric control design and actuator placement, AIAA J. 35 (3) (1997) 534–539.
[10] G. Overton, K. Worden, Sensor optimisation using an ant colony metaphor, Strain 40 (2) (2004) 59–65.
[11] E.M. Hernandez, Efficient sensor placement for state estimation in structural dynamics, Mech. Syst. Sig. Process. 85 (2017) 789–800.
[12] A. Bay, D. Carrera, S.M. Fosson, P. Fragneto, M. Grella, C. Ravazzi, E. Magli, Dictionary design for sensor network localization via block-sparsity, IEEE, 2015 IEEE 17th International Workshop on Multimedia Signal Processing (MMSP), 2015.
[13] J. Shen, S. Mousavi, Least sparsity of p-Norm based optimization problems with p > 1, SIAM J. Optim. (2018) 2721–2751.
[14] R.F. Guratzsch, S. Mahadevan, Structural health monitoring sensor placement optimization under uncertainty, AIAA J. 48 (7) (2010) 1281–1289.
[15] P.F. Wang, Z.Q. Wang, B.D. Youn, S. Lee, Reliability-based robust design of smart sensing systems for failure diagnostics using piezoelectric materials, Comput. Struct. 156 (2015) 110–121.
[16] R. Castro-Triguero, S. Murugan, R. Gallego, M.I. Friswell, Robustness of optimal sensor placement under parametric uncertainty, Mech. Syst. Sig. Process. 41 (1–2) (2013) 268–287.
[17] L. Vincenzi, L. Simonini, Influence of model errors in optimal sensor placement, J. Sound Vib. 389 (2017) 119–133.
[18] S.S. Dhillon, K. Chakrabarty, Sensor placement for effective coverage and surveillance in distributed sensor networks, in: IEEE Wireless Communications and Networking Conference, 2003, pp. 1609–1614.
[19] P.H. Kirkegaard, R. Brincker, On the optimal location of sensors for parametric identification of linear structural systems, Mech. Syst. Sig. Process. 8 (6) (1994) 639–647.
[20] B.B. Li, A.D. Kiureghian, Robust optimal sensor placement for operational modal analysis based on maximum expected utility, Mech. Syst. Sig. Process. 75 (2016) 155–175.
[21] J. Lee, F.J. Wu, W.Y. Zhao, M. Ghaffari, L.X. Liao, D. Siegel, Prognostics and health management design for rotary machinery systems-reviews, methodology and applications, Mech. Syst. Sig. Process. 42 (1–2) (2014) 314–334.
[22] R. De Maesschalck, D. Jouan-Rimbaud, D.L. Massart, The Mahalanobis distance, Chemom. Intell. Lab. Syst. 50 (1) (2000) 1–18.
[23] B. Zhang, S.N. Srihari, Fast k-nearest neighbor classification using cluster-based trees, IEEE Trans. Pattern Anal. Mach. Intell. 26 (4) (2004) 525–528.
[24] K. Alsabti, S. Ranka, V. Singh, An efficient k-means clustering algorithm, Electr. Eng. Comput. Sci. (1997).
[25] P.F. Wang, B.D. Youn, C. Hu, J.M. Ha, B. Jeon, A probabilistic detectability-based sensor network design method for system health monitoring and prognostics, J. Intell. Mater. Syst. Struct. 26 (9) (2015) 1079–1090.
[26] T. Nguyen, T.H.T. Chan, D.P. Thambiratnam, Controlled Monte-Carlo data generation for statistical damage identification employing Mahalanobis squared distance, Struct. Health Monit. 13 (4) (2014) 461–472.
[27] T. Nguyen, T.H.T. Chan, D.P. Thambiratnam, Field validation of controlled Monte Carlo data generation for statistical damage identification employing Mahalanobis squared distance, Struct. Health Monit. 13 (4) (2014) 473–488.
[28] A.A. Mosavi, D. Dickey, R. Seracino, S. Rizkalla, Identifying damage locations under ambient vibrations utilizing vector autoregressive models and Mahalanobis distances, Mech. Syst. Sig. Process. 26 (2012) 254–267.
[29] Y. Kim, J.W. Chong, K.H. Chon, J. Kim, Wavelet-based AR-SVM for health monitoring of smart structures, Smart Mater. Struct. 22 (1) (2013).

[30] T.W. Simpson, A.J. Booker, D. Ghosh, A.A. Giunta, P.N. Koch, R.J. Yang, Approximation methods in multidisciplinary analysis and optimization: a panel discussion, Struct. Multidiscip. Optim. 27 (5) (2004) 302–313.
[31] C. Currin, T. Mitchell, M. Morris, D. Ylvisaker, Bayesian prediction of deterministic functions, with applications to the design and analysis of computer experiments, J. Am. Stat. Assoc. 86 (416) (1991) 953–963.
[32] T.W. Simpson, F. Mistree, Kriging models for global approximation in simulation-based multidisciplinary design optimization, AIAA J. 39 (12) (2001) 2233–2241.
[33] S. Jeong, M. Murayama, K. Yamamoto, Efficient optimization design method using kriging model, J. Aircraft 42 (2) (2005) 413–420.
[34] M.K. Sadoughi, M. Li, C. Hu, C.A. MacKenzie, S. Lee, A.T. Eshghi, A high-dimensional reliability analysis method for simulation-based design under uncertainty, J. Mech. Des. 140 (7) (2018) 12.
[35] J.J. Warnes, B.D. Ripley, Problems with likelihood estimation of covariance functions of spatial gaussian-processes, Biometrika 74 (3) (1987) 640–642.
[36] E. Brochu, V.M. Cora, N. De Freitas, A tutorial on Bayesian optimization of expensive cost functions, with application to active user modeling and hierarchical reinforcement learning, arXiv preprint arXiv:1012.2599, 2010.
[37] M. Sadoughi, C. Hu, C.A. Mackenzie, A. Toghi Eshghi, S. Lee, Sequential exploration-exploitation with dynamic trade-off for efficient reliability analysis of complex engineered systems, Structural and Multidisciplinary Optimization, Springer, 2017.
[38] M.D. McKay, R.J. Beckman, W.J. Conover, A comparison of three methods for selecting values of input variables in the analysis of output from a computer code, Technometrics 21 (2) (1979) 239–245.
[39] A.T. Eshghi, S. Lee, M.K. Sadoughi, C. Hu, Y.C. Kim, J.H. Seo, Design optimization under uncertainty and speed variability for a piezoelectric energy harvester powering a tire pressure monitoring sensor, Smart Mater. Struct. 26 (10) (2017) 18.
[40] A. Toghi Eshghi, S. Lee, Y.-C. Kim, Design under uncertainty for a piezoelectric energy harvester to power a tire pressure monitoring system, ASME, 29th Conference on Mechanical Vibration and Noise, 2017.
[41] A. Toghi Eshghi, S. Lee, M.K. Sadoughi, C. Hu, Y.-C. Kim, J.-H. Seo, Experimental verification of tire energy harvester designed via reliability based design optimization method, Active and Passive Smart Structures and Integrated Systems XII, International Society for Optics and Photonics, 2018.